https://doi.org/10.5194/egusphere-2026-805
Preprint. Discussion started: 17 February 2026


# MAJIS performances in the infrared during the JUICE 2024 Earth fly-by: comparisons with IASI measurements and sensitivity to trace species

Sandrine Guerlet[1,2], Raymond Armante[1], Ninon Lauzanne[1], François Poulet[3], Yves Langevin[3], Sébastien Rodriguez[4], Leigh Fletcher[5], Thierry Fouchet[2], Giuseppe Piccioni[6], and Alessandra Migliorini[7]

[1]Laboratoire de Meteorologie Dynamique, LMD-IPSL, CNRS, Sorbonne Université, Université PSL, Institut Polytechnique, Paris, France
[2]LIRA, Observatoire de Paris, Université PSL, CNRS, Sorbonne Université, Université Paris Cité, 92195 Meudon Cedex, France
[3]IAS, CNRS, Université Paris-Saclay, 91405 Orsay Cedex, France
[4]Université Paris Cité, Institut de physique du globe de Paris (IPGP), CNRS, Paris, France
[5]School of Physics and Astronomy, University of Leicester, Leicester, United Kingdom
[6]Istituto Nazionale di Astrofisica - Istituto di Astrofisica e Planetologia Spaziali (INAF-IAPS), I-00133, Roma, Italy
[7]Istituto Nazionale di Astrofisica - Astronomical Observatory of Padova, I-35122, Padova, Italy

**Correspondence:** Sandrine Guerlet (sandrine.guerlet@lmd.ipsl.fr)

**Abstract.** The JUpiter ICy moons Explorer spacecraft (JUICE) successfully performed a Lunar and Earth gravity assist maneuver on 19 and 20th August 2024, which provided an excellent opportunity to test its instruments before its arrival at Jupiter in 2031. Here we focus on the evaluation of the performances of the infrared channel of the Moon and Jupiter Imaging Spectrometer (MAJIS) based on Earth observations acquired over part of the Pacific Ocean at tropical latitudes. We specifically compare MAJIS observations with co-located ones from the Infrared Atmospheric Sounding Interferometer (IASI). The two instruments overlap in the spectral range 3.6 and 5.56 $\mu$m. Having removed spectra contaminated by clouds or ocean glint, we find an excellent match between the absolute radiance of the two instruments. We argue that most of the differences can be explained by natural variability of water vapour content. Once this effect is taken into account, our results suggest that the radiometric calibration of MAJIS is better than 10%, rising to $\sim$15% in the range 5.25–5.56 µm. We then compare MAJIS to synthetic spectra generated with a radiative transfer algorithm, the OPerational version of the Automatized Atmospheric Absorption Atlas (4A/OP). Both the comparison of MAJIS to IASI and to synthetic spectra reveal a small spectral shift of MAJIS spectra beyond 4 µm, of the order of 4 nm. The use of 4A/OP allows us to highlight the detection and sensitivity of MAJIS spectra to several trace species: methane ($CH_4$), nitrous oxide ($N_2O$), ozone ($O_3$) and carbone monoxide (CO). Based on the residuals between MAJIS and synthetic spectra, we estimate the signal-to-noise ratio to lie in the range 200–300, meeting nominal expectations. These excellent performances point to promising future jovian atmospheric observations.

https://doi.org/10.5194/egusphere-2026-805
Preprint. Discussion started: 17 February 2026


## 1 Introduction

The Jupiter Icy Moons Explorer, launched in April 2023, performed a successful Lunar and Earth gravitational assist on 19 and 20 August 2024, which provided a unique opportunity to test the in-flight performances of its instruments. Here we specifically address the observations of the Earth performed by the Moons And Jupiter Imaging Spectrometer (MAJIS). This instrument is equipped with two channels: one covering the visible and near-infrared (0.5–2.35 µm) and the other covering the infrared (2.28–5.56 µm). Detailed characteristics of the MAJIS instrument can be found in Poulet et al. (2024). During the fly-by, MAJIS recorded spectra of the Earth surface (mostly the ocean) and atmospheric thermal emission and solar back scattered radiation over part of East Asia and the Pacific Ocean (see Poulet et al. (2025) for an overall description of the Earth fly-by). With several remote sensing satellites dedicated to Earth observation, we took this opportunity to compare MAJIS spectra with those taken from the Infrared Atmospheric Sounding Interferometer (IASI, Phulpin et al. (2007)) at similar locations, local times and viewing angles. IASI records spectra of the Earth thermal emission and solar reflection in the range 3.6–15.5 µm and is known for its excellent performances in terms of absolute radiometric calibration, spectral calibration and signal-to-noise ratio. Indeed, IASI measurements have been themselves validated against ground-based observations (Armante et al., 2016) and are often used as a reference to cross-calibrating other remote sensing instruments (Larar et al., 2010).

As MAJIS and IASI overlap in their spectral coverage between 3.6 and 5.56 $\mu$m, we focus in this paper on the evaluation of the radiometric and spectroscopic calibration of MAJIS IR channel by comparing its measurements with co-located IASI observations. To interpret small differences between instruments, we use a radiative transfer model, 4A/OP (Scott and Chedin, 1981; Cheruy et al., 1995), that is also used to assess the spectroscopic calibration of MAJIS spectra (see Langevin et al. (2026) for details about calibration). As one goal of MAJIS is to retrieve and map the concentration of several trace species in Jupiter's atmosphere (e.g. water, ammonia, phosphine; see Fletcher et al. (2023)), we use the Earth fly-by as an opportunity to test the sensitivity of the instrument to trace species in the Earth's atmosphere, namely methane ($CH_4$), ozone ($O_3$), carbon monoxide (CO) and nitrous oxide ($N_2O$). The radiative transfer code is described first, in section 2, then the characteristics of IASI are detailed in section 3. The co-location method with IASI and the resulting comparison of the two datasets are presented in section 4. Results on the sensitivity of MAJIS to trace species are detailed in section 5.

## 2 Description of 4A/OP

4A/OP, standing for OPerational version of the Automatized Atmospheric Absorption Atlas, is a fast and accurate radiative transfer model developed by the Laboratoire de Météorologie Dynamique (LMD), the French Centre National d'Etudes Spatiales (CNES) and Noveltis (see Dogniaux et al. (2021) and references therein). This model exploits pre-built computations of optical thicknesses in the form of "Atlases", generated at a spectral resolution of $5\times10^{-4}$ cm$^{-1}$ and for various reference temperature-pressure profiles representative of the Earth atmospheric variations. To calculate the optical thicknesses, spectroscopic parameters are nominally provided from the latest version of GEISA spectroscopic database (Jacquinet-Husson et al., 2016; Delahaye et al., 2021). Developed initially for the thermal infrared region, 4A/OP has been adapted to the shortwave infrared and visible range. It is a flexible code that can accommodate different types of geometries (nadir, limb, occultation),

https://doi.org/10.5194/egusphere-2026-805
Preprint. Discussion started: 17 February 2026


user-defined instrument response functions, up to 53 molecules, and the possibility to include scattering by clouds and aerosols (Sic et al., 2026). Derivatives of the radiance with respect to temperature or mixing ratio of a species (Jacobians) can also be calculated. For example, 4A/OP is used for the daily retrievals of sea surface temperature and trace species from IASI and has been selected by CNES as the reference radiative transfer model for the development of the MicroCarb and MERLIN missions (Cassé et al., 2021).

In the following, we generate spectra in the thermal infrared part (2.5 to 5.5 µm for MAJIS; 3.6 to 15.5 µm for IASI) and neglect scattering. We will consider only cloud-free scenes (see section 4.1) and thus omit emission and absorption by clouds. Data considered here were acquired over the ocean: marine aerosols are most likely present, but their extinction is negligible in the thermal infrared and is not included either. The ocean emissivity is set to 0.98 for the whole spectral range considered here. The radiative transfer code considers 43 vertical layers in plane-parallel approximation, the first one just above the surface and the uppermost layer located at $2.5\times10^{-3}$ hPa. Molecules considered in the radiative transfer calculations are $H_2O$, $CO_2$, $O_3$, $N_2O$, CO, $CH_4$, $O_2$, NO, HDO for MAJIS calculations as well as $SO_2$, $NO_2$, $C_2H_6$, $C_2H_2$, $NH_3$ and three CFC for IASI studies. In addition, several continua and Collisional Induced Absorption (CIA) emissions are taken into account ($N_2$, $O_2$, $H_2O$), as well as line-mixing effects for $CO_2$, $CH_4$ and $H_2O$.

Regarding the instrument function, for MAJIS we assume a Gaussian shape with a nominal full width at half maximum (FWHM) of 6.86 nm, as determined from ground-based spectral calibration (Haffoud et al., 2024), while the IASI FWHM is defined in wavenumbers units and amounts to 0.50 $cm^{-1}$ (corresponding to a FWHM of 1.25 nm at 5 µm).

## 3 Characteristics of IASI observations

IASI is a Fourier Transform infrared spectrometer mounted onboard each of the three EUMETSAT Meteorological Operational satellite MetOp-A, B and C satellites launched respectively in 2006, 2012 and 2018. The Metop-A instrument stopped operating in 2021 but IASI is still operating on MetOp-B and C as we write this manuscript. Initially dedicated to the meteorological monitoring of atmospheric temperature, water vapour (August et al., 2012) and surface temperature (Capelle et al., 2022), IASI has demonstrated is capability to monitor also the atmospheric composition such as carbon dioxide, methane (Crevoisier et al., 2009, 2013), ammonia and halogenated species (Clerbaux et al., 2009). Spectral emissivity and aerosol opacity can be retrieved as well from IASI spectra (Capelle et al., 2014). IASI covers the spectral region between 645 and 2760 $cm^{-1}$ (3.4 and 15.6 $\mu$m) with a spectral resolution of 0.5 $cm^{-1}$ (apodized). This corresponds to a spectral resolution R of 4000 at 5 µm, about six times higher than MAJIS. Its field of view is composed of $2\times2$ circular pixels, corresponding to a 12 km diameter individual footprint on Earth, at nadir. This is considerably larger than the $\sim$1.3 km spatial resolution of an individual MAJIS pixel projected on Earth, under the conditions of the JUICE's Earth flyby of August 2024. The MetOp satellites are on polar Sun-synchronous orbits, observing the Earth near 9:30 and 21:30 local time (at nadir). The IASI instruments scan the Earth across the satellite's tracks with a swath of $\pm48°$ around nadir. With an orbital period of approximately 2 hours, global coverage is reached in 12 hours. For comparison, MAJIS Earth observations spanned aproximately the local time range 3:00–10:30 (see also Oliva et al. (2026) for full information on local times and geometries of MAJIS Earth scans).

https://doi.org/10.5194/egusphere-2026-805
Preprint. Discussion started: 17 February 2026


An example of a IASI spectrum on its full wavelength range is shown in Fig. 1, along with a synthetic spectrum that we computed with 4A/OP. This example was chosen among the IASI-MAJIS co-located data discussed later. We did not perform any retrievals in this paper; rather, this synthetic spectrum was generated by setting the main parameters (surface temperature, atmospheric temperature, humidity profiles) to the Level 2 IASI data (EUMETSAT data products, August et al. (2012)). The ozone profile was set to that extracted from the ERA5 reanalysis for this time and location and was slightly scaled to match the ozone band at 9.6 µm. Other trace species were set to typical vertical profiles found in the tropics. For CO, $CH_4$ and $N_2O$, we further scaled these profiles in order to obtain a best fit of the corresponding spectral features. This set of trace species profiles will serve as a basis for our sensitivity studies in section 5.

The excellent agreement between the model (4A/OP) and the IASI observations shown in Fig. 1 vouch for the use of the 4A/OP radiative transfer model in our study. We note however that the synthetic spectrum underestimates the emission in the core of the 4.3 µm $CO_2$ band, which is a well-known shortcoming of several radiative transfer models (including 4A/OP) that do not take into account the complex contribution from non-LTE $CO_2$ emission, originating from the upper stratosphere. We also notice a very small overestimation of radiance in the 4A/OP spectrum in the range 3.6–4.0 µm and 8–9 µm, and an underestimation of the observed radiance in the range 10–12 µm. This mismatch, here on the order of 0.05 W/m$^2$/sr/µm, is not systematic among the various IASI measurements we analysed. We suspect that it could be due to the assumption of a constant emissivity over the whole spectral range in our simulations, while the actual emissivity is slightly wavelength and viewing angle dependent.

## 4 Comparison of IASI and MAJIS co-located data

In the following, we present our methodology to match IASI and MAJIS data according to several criteria (cloud filters, spatio-temporal criteria, viewing geometry, etc). While 19 data cubes were acquired by MAJIS in the range of longitudes 80–190E (see Poulet et al. (2025) for a full projected map), we will present detailed results for only 11 of these data cubes : we exclude the last one, acquired in near limb geometry, and do not show the results for 7 other cubes taken at longitudes west of 120°E as the local time difference with IASI is too significant (3 to 6 hours). The 11 MAJIS data cubes selected at this stage (Fig. 2) were all acquired in early morning, between ∼6h00 and 10h30.

### 4.1 Filtering for clouds

Before searching for co-located data, a first step is to filter out cloudy observations from both datasets. Indeed, the precise local time, location and size of the footprints of the two instruments being different, they could be contaminated by clouds in different ways. Clouds, located in the troposphere, are much colder than the surface and appear as a low radiance thermal emission. Even a small contamination by cloud will impact the outgoing emission spectra (see also Poulet et al. (2025); Oliva et al. (2026)). The brightness temperature (BT) near 3.9 µm or 4.6 µm serves as good proxy for cloud coverage in the thermal infrared, in particular above the tropical ocean where the surface temperature does not vary significantly over large areas. At these wavelengths, located in regions of small gaseous opacity, a low BT will indicate the presence of tropospheric clouds,

https://doi.org/10.5194/egusphere-2026-805
Preprint. Discussion started: 17 February 2026


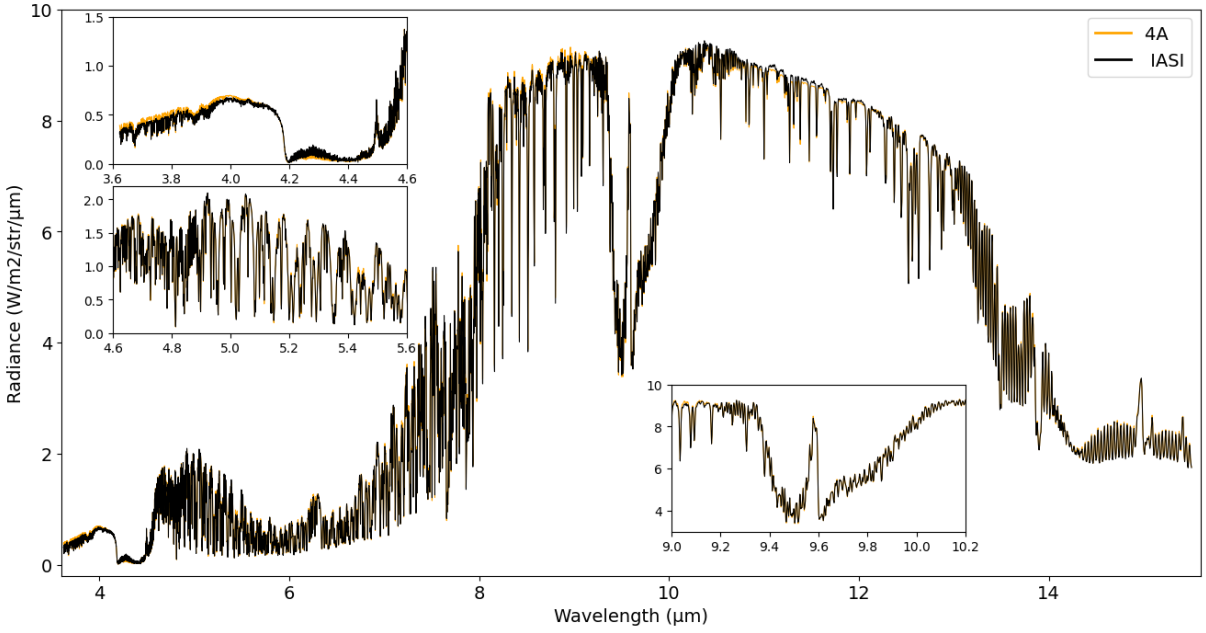


**Figure 1.** Example of a IASI spectrum acquired over the Pacific Ocean on 20 August 2024 (in black) along with a synthetic spectrum generated with 4A (orange). Embedded are three zooms, one centered at the 9.6 µm ozone band as a showcase of excellent agreement between model and observations, and two others covering MAJIS spectral range to highlight the complex spectral features in this range.

emitting infrared radiation at cold temperatures. A map of the BT at 4.6 µm for both MAJIS and IASI observations is shown in Fig. 2, revealing a few cloudy areas. A striking feature appears for MAJIS observations labeled 'C12', 'C13' and 'C14', that have much lower BT than the surroundings and than the crossing MAJIS observation labeled 'C11'. This cannot be explained by cloud cover; rather, these three MAJIS observations were acquired with a twice longer integration time and the signal saturates, affecting MAJIS spectra in the range 4.5–5.2 µm. While these three data cubes appear for context in some of the following figures, they will not be retained in the final selection of MAJIS-IASI colocated data.

To filter out for clouds, on the MAJIS side, we rule out spectra that have a brightness temperature at 4.64 µm lower than 290K. This threshold is justified by a visual inspection of the data in both the thermal infrared at 4.64 µm and in the visible at 0.7 µm, as shown in Fig. 3. Indeed, bright areas at 0.7 µm indicate the presence of reflective clouds on top of a dark albedo ocean, and are strongly correlated with low brightness temperatures. Examples of MAJIS spectra for cloudy or cloud-free pixels are shown in Fig. 4 to illustrate this effect. On the IASI side, level 2 data come with a cloud fraction value within the IASI footprint, estimated from an onboard camera. We choose to keep IASI data with a cloud fraction less than 5%, which is small enough to not significantly affect the outgoing thermal emission. In addition, we note that all IASI pixels flagged as cloud-free have indeed brightness temperatures higher than ∼290K at 4.64 µm, which validates our chosen threshold for MAJIS (see Fig. 5).

https://doi.org/10.5194/egusphere-2026-805
Preprint. Discussion started: 17 February 2026


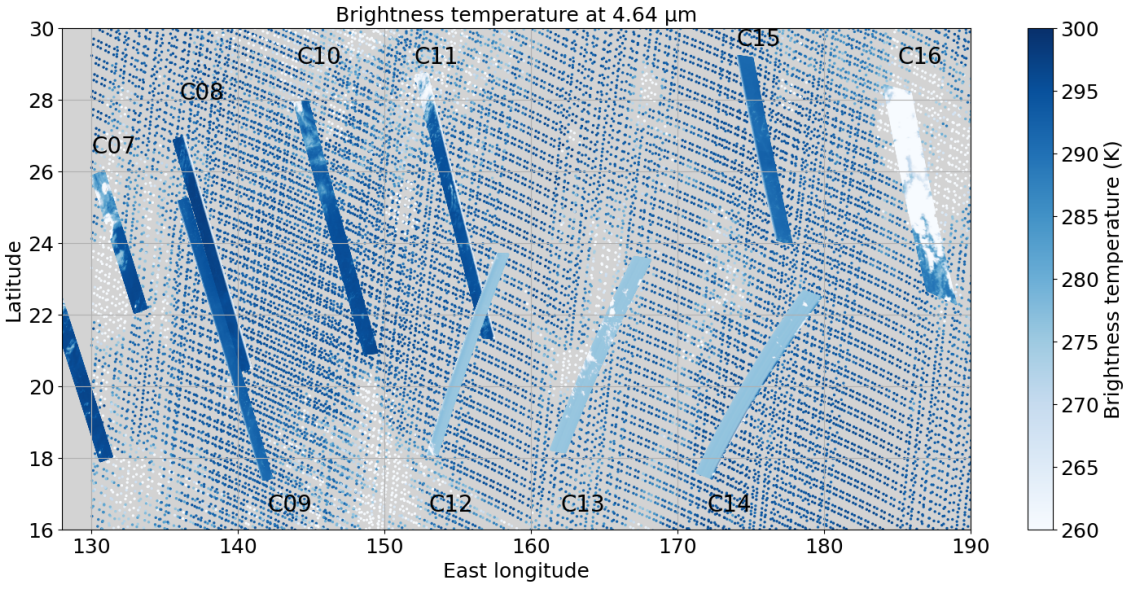


**Figure 2.** Map of the brightness temperature at 4.64 µm for 11 MAJIS swaths, used as a proxy for clouds. All small dots represent brightness temperature for IASI observations (same color range). Each MAJIS swath is 64 pixels wide and approximately 500 pixel long. Labels are the same as thos used in Oliva et al. (2026). Swaths labeled 'C12', 'C13' and 'C14' appear colder due to a saturation effect (see text).

### 4.2 Effect of the glint spot

We further exclude, from our co-location analyses, IASI and MAJIS data contaminated by the specular reflection of the Sun over the ocean, which is called the glint spot. This occurs when the solar zenith angle is close to the satellite viewing zenith angle, and is also highly sensitive to the viewing azimuth angle. Indeed, as the ocean is not a smooth surface, the strength and direction of specular sunlight reflection depends on the orientation and slopes of the waves, acting as many small surfaces reflecting sunlight in a very directionnal manner. The main contribution of this solar specular reflection is found in the visible range (hence in the VIS channel of MAJIS), but it also features a signature in the range 3.4–4 µm (see Fig. 6), hence present in both IASI data and MAJIS NIR channel. A study of the Sun specular reflection signal in IASI observations can be found in Guérin et al. (2023), which reports on how the wind strength and direction changes the orientation of the wave facets, hence the strength of this signal. As a result, we notice that two observations (one by IASI, one by MAJIS) can be very close in space and time, have similar viewing zenith angles, but be affected very differently by solar specular reflection, having different azimuth viewing angles.

In MAJIS (daylight) observations, one straightforward way to discard observations within the glint spot is to search for anomalously high radiance in the near infrared (in the VISNIR channel of MAJIS), where the ocean albedo is dark and any significant signal has to be a reflection from a cloud and/or the glint spot. A map of MAJIS radiance at 2.35 µm is shown in Fig. 7 to illustrate this effect, revealing that swaths labeled from 'C12' to 'C15' are contaminated by solar specular reflection.

https://doi.org/10.5194/egusphere-2026-805
Preprint. Discussion started: 17 February 2026


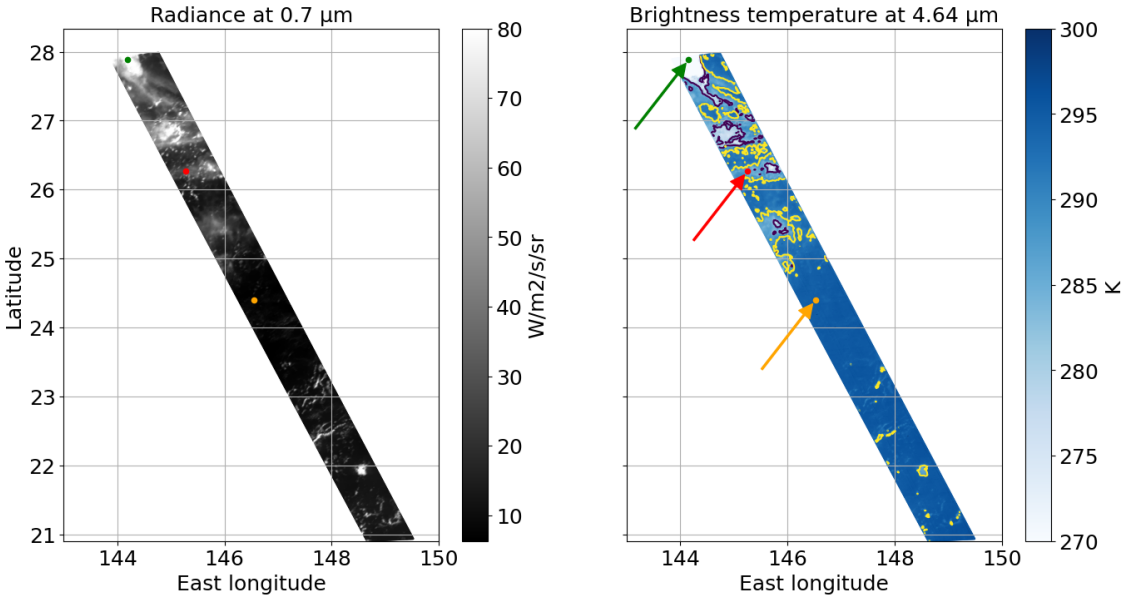


**Figure 3.** MAJIS radiance in the visible at 0.7 µm (left) and brightness temperature at 4.64 µm (right) for the swath labeled 'C10' in Fig. 2. On the right panel, the purple contour highlight BT values lower than 282K, the yellow contour BT values of 290K. Patches of clouds visible in the left panel are well identified by their low BT values in the right panel. Three dots (in green, red and orange) highlight three pixels which spectra are shown in Fig. 4.

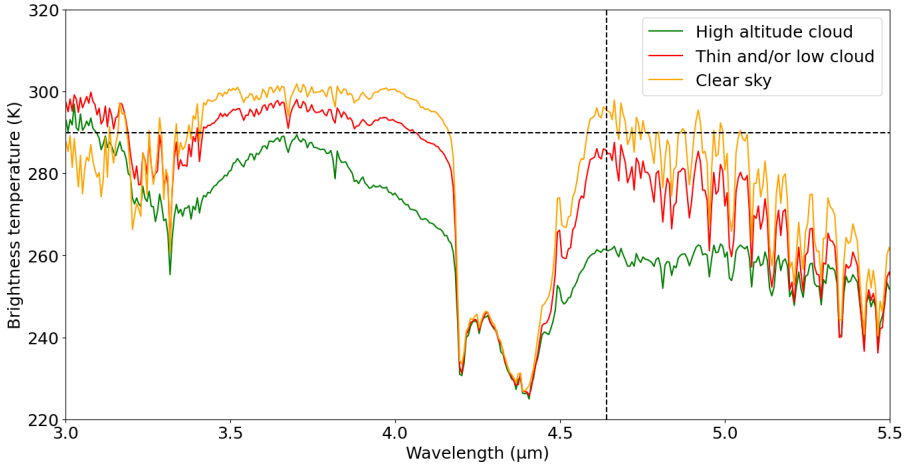


**Figure 4.** MAJIS spectra, in brightness temperature units, for three pixels from swath labeled 'C10' highlighted in color in Fig. 3. Dashed lines indicate the threshold value of 290K at 4.64 µm: spectra below this threshold are considered cloudy.

For instance, swath labeled 'C15' was considered mostly cloud-free based on the BT at 4.64 µm but exhibits a non-zero radiance at 2.35 µm over a large part of its swath. This is consistent with the close values, for this data cube, of solar zenith

https://doi.org/10.5194/egusphere-2026-805
Preprint. Discussion started: 17 February 2026


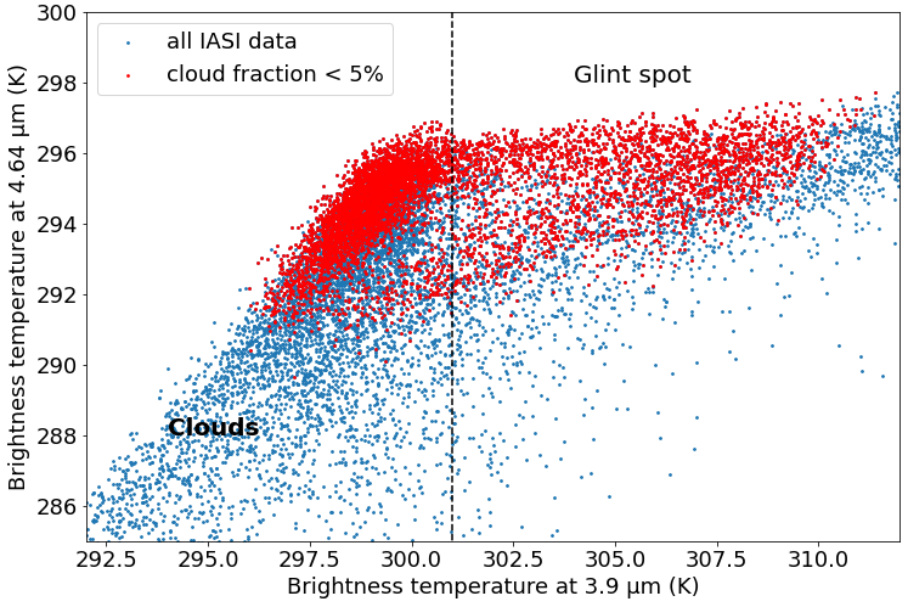


**Figure 5.** Scatter plot of the BT at 4.64 µm versus that at 3.9 µm for all IASI observations. Data colored in red have a negligible cloud coverage (less than 5%) within their field of view, as determined by an onboard camera. These cloudfree observations are clustered near BT values of 292–297 K at 4.64 µm and 296–301K at 3.9 µm. The "tail" of high BT at 3.9 µm (>301K) represents observations with significant contribution from the specular reflection of the Sun (glint spot).

angles (41°) and viewing angles (49°). On the other hand, 'C08' and 'C09' are considered cloud-free and are also dark at 2.35 µm, hence not contaminated by glint.

However, this criterion cannot be applied to IASI, as its spectral coverage only starts at 3.6 µm. We therefore use the 3.9 µm signal as a proxy for glint contamination, as this wavelength lies in a relatively transparent spectral region (low gaseous opacity) and its intensity correlates well with excess radiance observed at shorter wavelengths in the MAJIS VISNIR channel. At this wavelength, in the absence of cloud, the radiance should more or less correspond to the ocean surface temperature (typically 298–300K), if the emission was that of a blackbody. When converted to brightness temperature (BT), however, the signal can reach values of up to 310K (see an example for IASI data in Fig. 5), which indicates the presence of additional non-thermal emission (in the form of solar specular reflection). Based on both the distribution of IASI BT distribution at 3.9 µm and the correlation of MAJIS BT at 3.9 µm and radiance at 0.7 µm, we decided to filter out data with a BT at 3.9 µm higher than 301K (see Fig. 5).

### 4.3 Co-location method

Once filtered for clouds, we searched for IASI data co-located with MAJIS observations according to several criteria: spatial coincidence, temporal coincidence, and similar viewing angles. The most stringent criteria is the temporal one, as IASI

https://doi.org/10.5194/egusphere-2026-805
Preprint. Discussion started: 17 February 2026


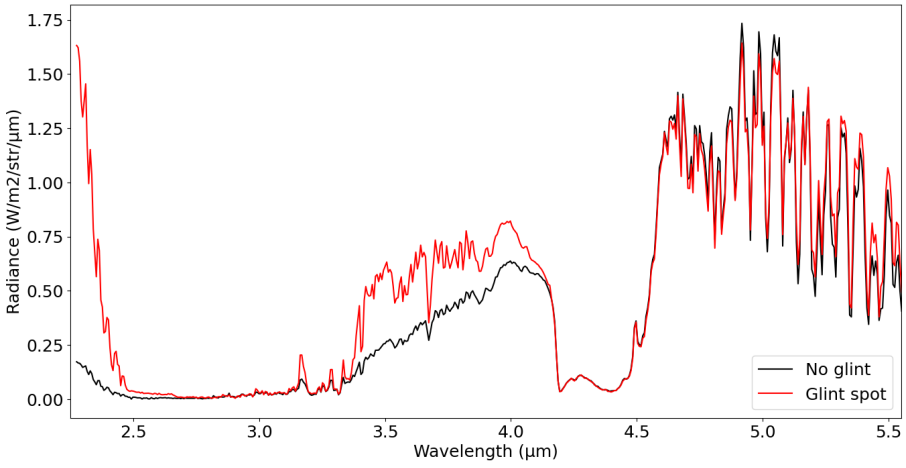


**Figure 6.** Example of two MAJIS spectra in the IR channel from swath labeled 'C15', inside (in red) and outside (in black) the glint spot.

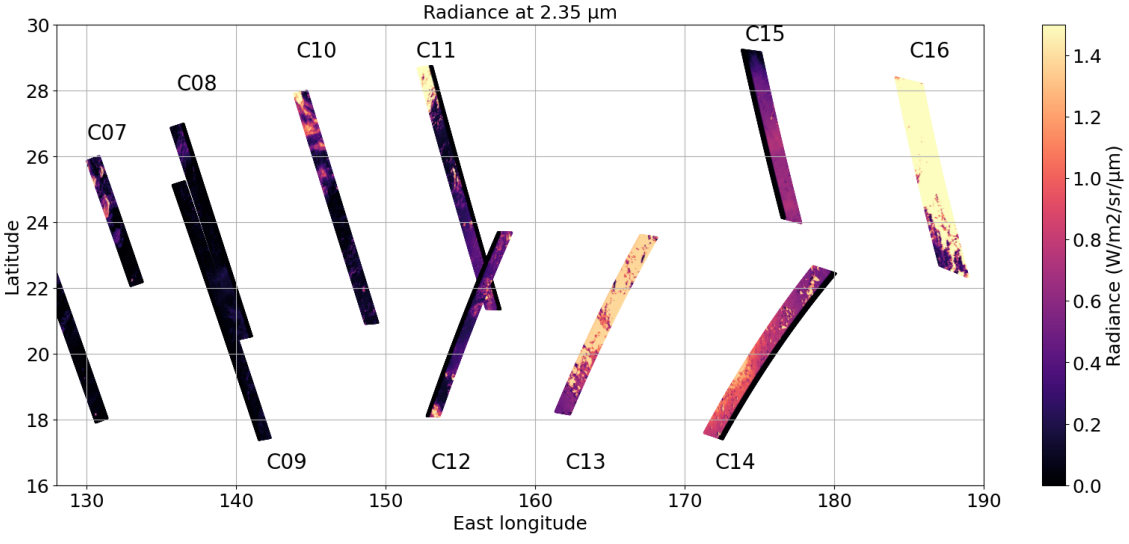


**Figure 7.** Map of the radiance at 2.35 µm from the VISNIR channel of MAJIS, capturing solar light reflected and backscattered by the surface and atmosphere. The ocean is very dark in the near infrared except in viewing geometries corresponding to the glint spot (specular reflection of the Sun) and/or in the case of reflection by clouds.

observations are acquired around very specific local times (9:30 AM, 9:30 PM). Fig. 8 shows the coverage of MAJIS and cloud-free IASI observations (both from the MetOp-B and MetOp-C satellites) in terms of local times. Setting a limit at $\pm 1$ hour and a difference in emission angle of $\pm 10°$ initially retains nearly a hundred IASI observations co-located with MAJIS data over the swaths labeled 'C14' and 'C15' (the former suffering from saturation). However, most of the MAJIS observations are contaminated by the glint spot here, leaving only 3 IASI spectra co-located with valid MAJIS ones. We thus extended the

https://doi.org/10.5194/egusphere-2026-805
Preprint. Discussion started: 17 February 2026


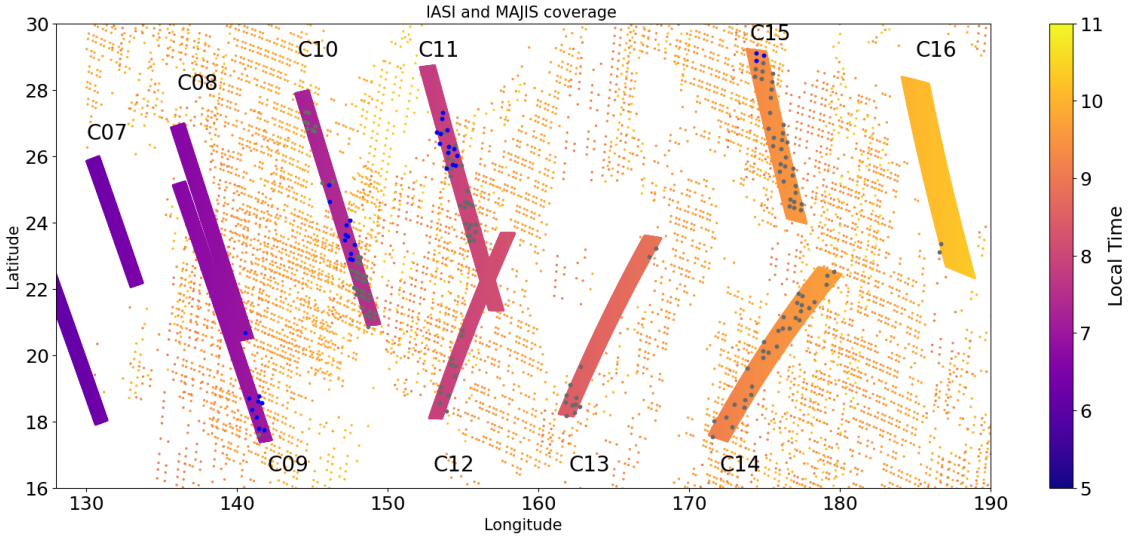


**Figure 8.** Projection of MAJIS observations, coloured according to local time. All dots represent the location of cloud-free IASI data (in orange as their local time is ∼9:30). Blue dots highlight all IASI data co-located with MAJIS that pass all quality filters. Grey dots are for cloud-free IASI data that did pass the spatial and temporal co-location criteria but either IASI or MAJIS was contaminated by glint (and/or MAJIS spectra were saturated).

**Table 1.** Summary of quality filters for IASI and MAJIS data, and co-location criteria.

| Criteria | IASI | MAJIS |
|---|---|---|
| Cloud | $<$ 5% cloud cover (camera) | BT(4.64 µm) $>$ 290K |
| Glint | BT(3.9 µm) $<$ 301K | |
| Diff. in emission angle | 20° | |
| Diff. in local time | 2.5 h | |
| Distance | MAJIS data within IASI footprint | |

criteria to ±2.5 hours and ±20° in emission angle and end up with 36 co-located IASI observations (blue dots in Fig. 8) not contaminated by clouds nor the glint spot. Each of these IASI observations is co-located with tens or even hundreds of MAJIS spectra. Indeed, for each IASI observation, we considered all MAJIS data contained into the much larger IASI field-of-view (see next section). The list of quality filters and co-location criteria are summarized in table 1.

### 4.4 Comparing IASI and MAJIS spectra

To quantitatively compare the two datasets, IASI spectra were convolved with the coarser 6.86 nm-wide FWHM of MAJIS. This initial comparison highlighted a small spectral shift between the two instruments beyond wavelengths of 4 µm, of the

https://doi.org/10.5194/egusphere-2026-805
Preprint. Discussion started: 17 February 2026


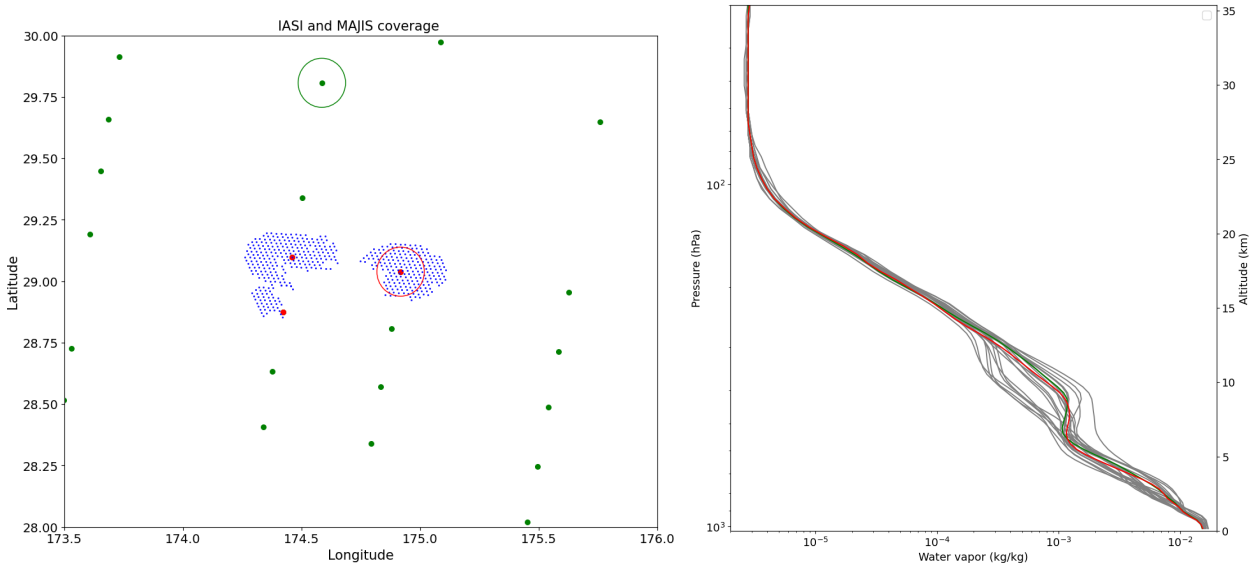


**Figure 9.** Left: Projection of MAJIS observations from swath 'C15' (in blue) situated within the approximate footprint of three co-located IASI observations whose central (latitude, longitude) are shown in red. The IASI footprint is not a circle but an ellipse due to a projection effect. Central coordinates for other IASI data in the surroundings are shown in green, used for contextual observations. Right: Vertical water vapour profiles corresponding to the 22 IASI observations shown on the left panel. The green and red profiles correspond to the location of two IASI data highlighted in the same colour (red and green circles) in the left panel.

order of 4 nm (less than a MAJIS spectral bin). Details of MAJIS spectral calibration and correction procedure can be found in Langevin et al. (2026); in the following, we will discuss results based on MAJIS spectra already corrected for this spectral shift.

Our best test cases are the three IASI spectra acquired on top of MAJIS swath 'C15': they were acquired less than 20 minutes away from MAJIS observations and with a 4° difference in emission angle (49° for MAJIS, 53° for IASI). A close-up on the spatial projection of the two datasets is shown in Fig. 9. Here we collected all MAJIS data situated within 0.12° of the centre of a IASI field of view (actually, within an ellipse elongated along the cross-track direction of IASI). We take into account the slight difference in emission angle by applying a correction factor to IASI spectra, based on the ratio of two synthetic spectra generated with 4A/OP for these two angles. The impact of this effect on the radiance is of the order of to 2–5%, depending on wavelength.

The raw comparison between IASI and MAJIS spectra is very satisfactory at first glance: we report absolute differences in radiance of the order of 0.15 W/m2/str/µm at maximum (see Fig. 10), MAJIS exhibiting lower radiances than IASI. This represents a 10% difference in relative value. Given that the surface temperature is not expected to change over the ocean over the 20-minutes time difference between the two acquisitions and that we strictly filtered out for clouds, we propose to take as a reference the near-transparent window near 4–4.1 µm. A correction of the order of +5% to MAJIS radiances would help reduce the MAJIS-IASI mismatch in that region, and could stem from a small bias in MAJIS absolute radiometric calibration.

https://doi.org/10.5194/egusphere-2026-805
Preprint. Discussion started: 17 February 2026


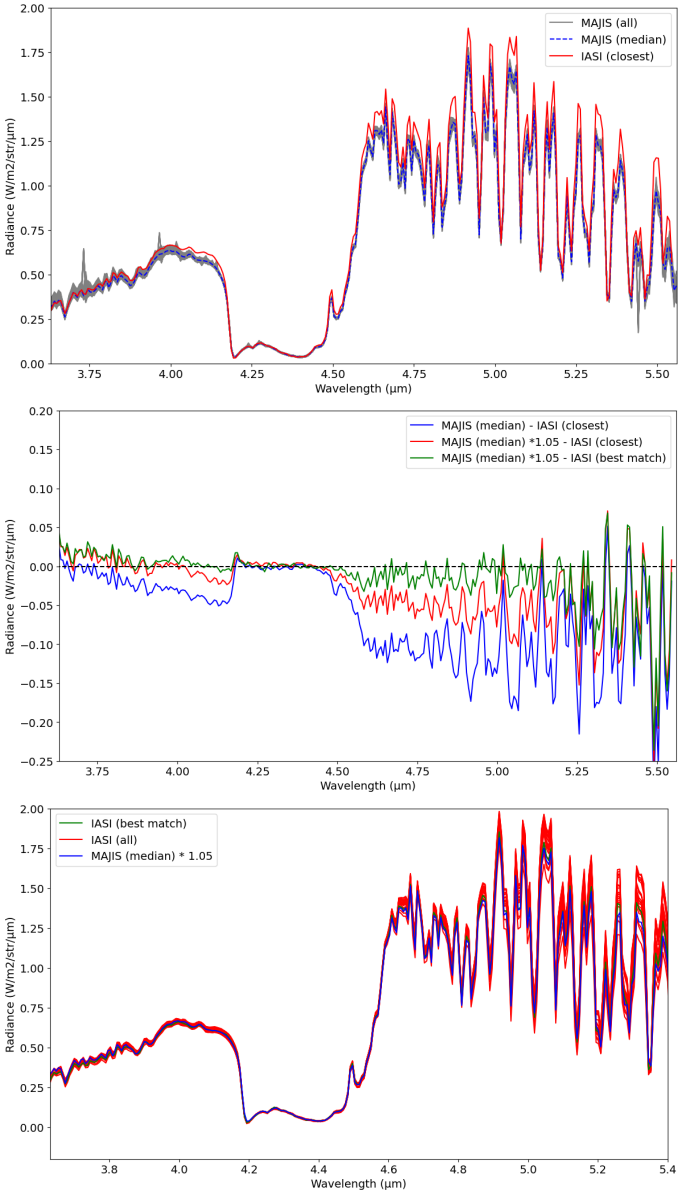


**Figure 10.** Top: Comparison of all of the MAJIS spectra co-located with one IASI observation (convolved to MAJIS resolution, in red). All 160 individual MAJIS spectra are plotted in grey, with the median plotted as a dashed blue line. Some hot pixels are visible as spikes in the individual MAJIS measurements. This example corresponds to the upper right case among the three red points in Fig. 9. Middle: Difference in radiance between the IASI spectrum shown in the top row and the median MAJIS spectrum (in blue), or considering the MAJIS spectrum multiplied by 1.05 (in red). In green is the MAJIS (multiplied by 1.05)-IASI difference using a nearby IASI observation (green spot in Fig. 9). Bottom: Comparison of 22 IASI spectra (convolved to MAJIS resolution), in red, in the surroundings of the same MAJIS observation (in blue, same as the top panel but multiplied by 1.05). The IASI spectrum that best matches the MAJIS one is highlighted in green.

https://doi.org/10.5194/egusphere-2026-805
Preprint. Discussion started: 17 February 2026


When applying this correction, MAJIS radiance becomes slightly greater than that of IASI at wavelengths <3.9 µm. This could be explained by a small residual contribution of the glint spot contaminating the MAJIS observation and not the IASI one, as discussed in section 4.2. However, applying this tentative +5% radiance to MAJIS spectra still does not fully bridge the gap between MAJIS and IASI in the range 4.5–5.5 µm (see bottom panel of Fig. 10). In this region, the MAJIS-IASI difference has significant peaks and troughs that cannot be explained by variations in the instrument FWHM. Rather, we propose that this mismatch is mainly caused by small differences in water vapour content between the two scenes. Indeed, this spectral region is dominated by water vapour absorption, which varies significantly even over small spatial scales. The right panel of Fig. 9 shows twenty-two water vapour profiles extracted from the Level 2 IASI data from the surroundings at the same time, and the twenty-two corresponding IASI spectra are displayed in the bottom of Fig. 10. We report a significant water vapour variability, of the order of ±50% in the middle troposphere, within 100 km of the central MAJIS observation considered here. We argue that the variability in radiance seen among those 22 IASI spectra mainly stems from changes in water vapour. Indeed, synthetic spectra generated with 4A/OP for these different water vapour profiles, with all other variables set fixed (surface and atmospheric temperatures) reproduces the variability observed in IASI spectra (not shown). We further note that our reference median MAJIS spectrum lies in the middle of the surrounding 22 IASI observations, once a +5% radiance correction is applied, which confirms the excellent MAJIS radiometric performance. We find that the MAJIS-IASI mismatch is significantly reduced if we consider a IASI observation slightly north of the MAJIS one (circled in green in Fig. 9, residuals shown in Fig. 10), having a slightly different water vapour profile. Such small changes in atmospheric humidity over the course of 20 minutes are plausible. This highlights the challenge of this inter-comparison exercise of two satellite datasets, even when strict co-location criteria are applied. Considering this "best match" (in green in Fig. 10), the final residual mismatch in the range 3.6–5.25 µm is now very small (<2%) and could be due to a combination of noise and/or small additional differences in water vapour and/or inaccuracies in our representation of the instrumental response function, these three components being difficult to disentangle.

In any case, we note that the mismatch remains significant beyond 5.25 µm, where MAJIS seems to systematically underestimate the radiance near the edge of the detector sensitivity, by ∼15–20%. We conclude from this detailed example that MAJIS radiometric calibration is better than 10% over most the range 3.6–5.25 µm and that there is a tentative low bias of the order of 5% in MAJIS observations. It is very challenging to make stronger and more precise statements about absolute calibration given the sensitivity to small variations in water vapour.

Looking at the other co-located spectra, the IASI-MAJIS agreement is also found to lie within 10%. We show an overview of the variations in radiance among both MAJIS and IASI spectra for swath labelled 'C10' and 'C11' in Fig. 11. Note that here, the local time difference with IASI is respectively 2h and 1h30, MAJIS observations being taken earlier in the morning. Another difference lies in the position of the field of view (FOV) of the MAJIS instrument: MAJIS physical array is 400-pixels wide, but during the Earth fly-by only a 64-pixel wide subset of the FOV acquired data: either the left edge of the detector (which was the case of swath labeled 'C15' in our study), the middle part (such as swath labelled 'C10') or the right edge (swath 'C11' here).

No correction factor has been applied to MAJIS in these figures; and the agreement between the two instruments seems excellent for swath 'C10'. One hypothesis is that MAJIS does have the same low 5% bias in radiance than that tentatively

https://doi.org/10.5194/egusphere-2026-805
Preprint. Discussion started: 17 February 2026


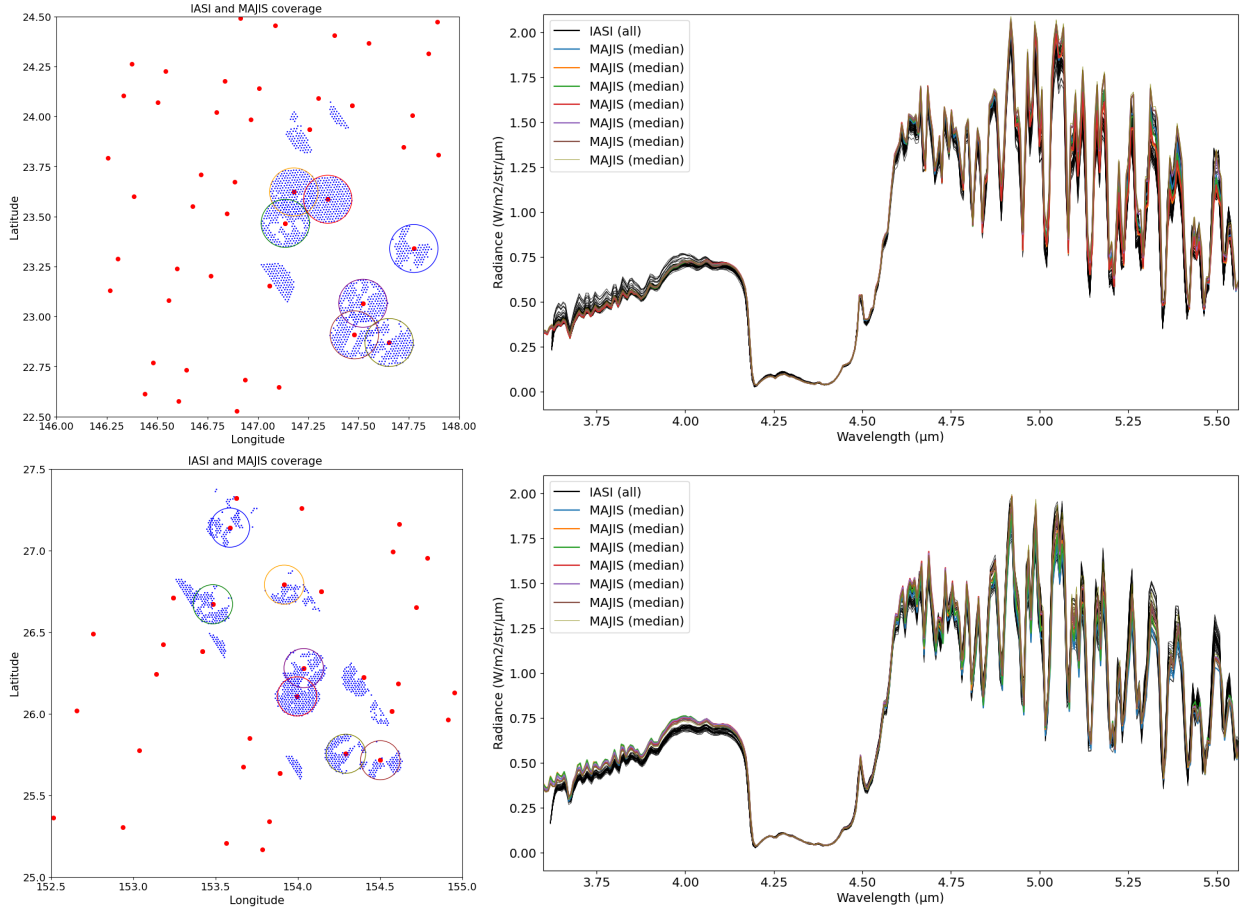


**Figure 11.** Left column: Projection of MAJIS observations (in blue) and IASI ones (in red). Right column: Comparison of IASI and MAJIS spectra. All IASI data present in each scene are plotted in black and the median of MAJIS data within each coloured circle is plotted according to the same colour code. The top row corresponds to observation swath labelled 'C10' (central pixels of the MAJIS array; local time difference with IASI of 2h), the bottom row to swath labelled 'C11' (right edge of the MAJIS array; local time difference with IASI of 1h30).

https://doi.org/10.5194/egusphere-2026-805
Preprint. Discussion started: 17 February 2026


determined above for swath 'C15', but there was less water vapour at this time of day, resulting in similar radiances than IASI (e.g., there is a compensation of errors). The other hypothesis is that there are no noticeable bias in MAJIS observations for its central pixels. Regarding swath 'C11', MAJIS radiance seems to be overestimated with respect to IASI for wavelengths $<4$ µm, hinting at a potential too high radiance bias on the right edge of the MAJIS detector, opposed to that tentatively derived at the left edge (swath 'C15'). Given the 2h time difference between IASI and MAJIS observations and potential variations in meteorological conditions, it is difficult to make a strong case for these potential biases. We note however that even if MAJIS radiometric calibration errors did depend on the position of the pixel on the array, these errors shall remain small ($<10\%$) (see also Langevin et al., this issue, for more details on that topic). This high-quality radiometric calibration has also been independently confirmed through the assessment and modeling of the lunar surface thermal contribution in MAJIS observations obtained during the Moon flyby (Tosi et al., 2025).

## 5 Comparison with synthetic spectra and sensitivity to trace species

Given the good agreement with IASI observations, we now turn to the detection of (and study of the sensitivity to) several trace species in MAJIS IR spectra: ozone, carbon monoxide, nitrous oxide and methane. To do so, we selected a pair of one IASI and one MAJIS individual measurement from our swath 'C15' where the minimum difference in radiance between the two datasets was found. We then defined a reference scenario (surface temperature, atmospheric temperature and composition vertical profiles) that best matches the IASI observation when computing the corresponding synthetic spectrum with 4A/OP. This reference atmosphere, based on the IASI L2 data, was already presented in section 3, along with the corresponding synthetic spectrum. We then computed another synthetic spectrum with the same surface and atmospheric conditions but for MAJIS spectral coverage and resolution. Hence, without running a retrieval, this method is expected to yield an excellent match to the MAJIS spectrum. The noise level was estimated from the variance of the residuals (MAJIS minus 4A/OP), excluding the core of the 4.2 µm $CO_2$ band where 4A/OP underestimated the radiance due to lack of non-LTE emission in the model. Signal-to-noise levels of the order of 200 to 300 are obtained, which is in the same range as the estimates given in Poulet et al. (2025). Note that similarly to the IASI-MAJIS comparison, the match between 4A/OP and MAJIS is poorer beyond 5.4 µm. We then successively generated similar spectra but without the contribution of a given trace species. We find that methane is detected to the level of 6 times the 1-$\sigma$ noise level, carbon monoxide to 4 times the noise level, ozone to 15 times the noise level, while nitrous oxide well exceeds these values (see Fig. 12).

To go further we then computed the Jacobians, which here are defined as the derivatives of the radiance at a wavelength $\lambda_i$ with respect to a change of 10% in concentration of a given trace species at an altitude $z_j$ (see Fig. 13). This allows for the determination of atmospheric layers for which the spectra have the greatest information content. This shows that we have the largest sensitivity to tropospheric $N_2O$, with a maximum sensitivity peaking at 500 hPa ($\sim$5km altitude); followed by stratospheric ozone, peaking at 30 hPa ($\sim$25–30 km altitude), while CO and $CH_4$ have a smaller absolute contribution and a broader peak in the troposphere (2–10 km). The Jacobians are negative : an increase in a trace species abundance will lead to a more pronounced absorption feature on top of the background (warmer) surface and lower atmosphere thermal emission. From

https://doi.org/10.5194/egusphere-2026-805
Preprint. Discussion started: 17 February 2026


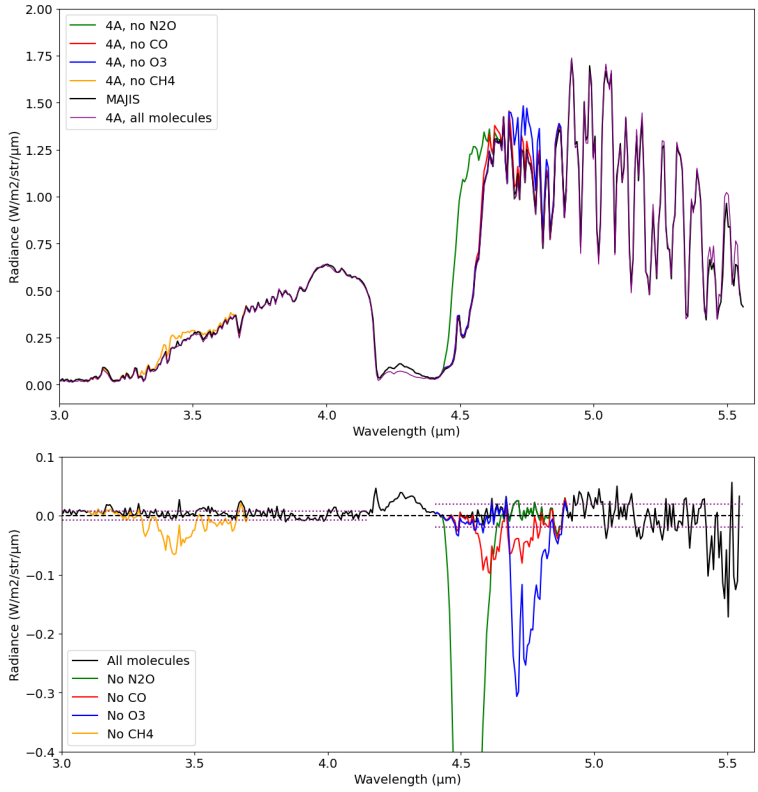


**Figure 12.** Top panel: Synthetic spectra generated with 4A/OP (color lines) compared to a MAJIS observation (in black), highlighting the sensitivity to several trace species. The bottom panel displays the residuals (MAJIS - 4A/OP). Estimate of the noise level in two spectral regions are displayed as dotted purple lines.

these Jacobians, we then computed the derivatives of the measurements to the total column of the trace species, which we call $K_C$. From the noise level at a given wavelength, $\sigma_i$, we can then compute the sensitivity $\sigma_C$ on the total column of each traces species that we can get from the measurements:

$$\sigma_C = \left( \sum_i \frac{K_{C,i}^2}{\sigma_i^2} \right)^{-\frac{1}{2}} \quad (1)$$

The sum is done over the wavelength range of a given emission band. Results are summarized in table 2 in terms of a fraction of the column. Based on MAJIS noise level, we find that the minimum uncertainty on the methane column is 14%, which is well above the typical observed column variations for this gas, which amount to ∼5%. Hence, no useful information on the $CH_4$ spatial variations can be derived from MAJIS spectra, which was expected : this methane band at 3.4 µm is scarcely used in Earth remote sensing owing to a low infrared signal at this wavelength in nadir and passive remote sensing observations (it is however exploited in limb geometry or with active, LIDAR techniques). A similar uncertainty is reached for carbon monoxide, which has a weak signature. Our greatest sensitivity is to $N_2O$ that can theoretically be derived with a 2.5% error on its column

https://doi.org/10.5194/egusphere-2026-805
Preprint. Discussion started: 17 February 2026


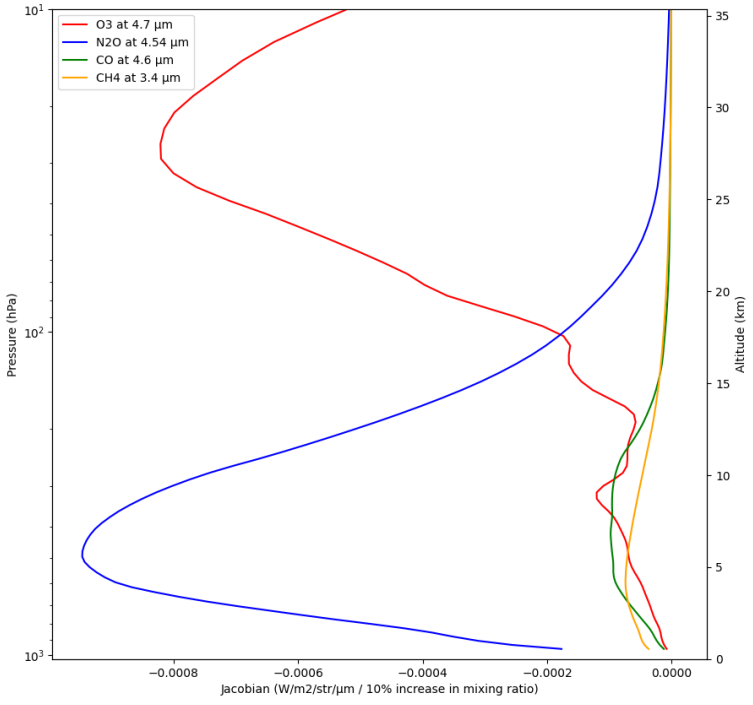


**Figure 13.** Impact on the radiance at a given wavelentgh (see label) to a change of 10%, at a given pressure level, in the mixing ratio of ozone (in red), nitrous oxide (blue), carbon monoxide (green) and methane (orange).

**Table 2.** Summary of the sensitivity study on trace species, based on the Jacobians and estimated noise level: peak altitude of the Jacobian, minimum uncertainty on the column abundance, in % ($\sigma_C/column * 100$), typical volume mixing ratio at this altitude, for the tropics, and typical range of observed variability.

| Molecule | peak altitude | uncertainty | typical concentration | typical variations |
|---|---|---|---|---|
| CO | 3–10 km | 14% | 100 ppbv | 20%* |
| $O_3$ | 25–30 km | 5% | 275 Dobson units | 10% |
| $N_2O$ | 3–8 km | 2.5% | 325 ppbv | 3% |
| $CH_4$ | 2–8 km | 14% | 1.8 ppmv | 5% |

* locally up to 250 ppbv, hence 100% variation and more, over forest fires.

followed by ozone, where we estimate our sensitivity to its integrated column to 5%. Note that our actual sensivitity would be to a partial column, as shown from Fig. 13. In addition, these estimates are "lower bound" values as the actual uncertainty would account for the propagation of several sources of errors (eg. on the temperature profile, ground emissivity,...) and for the correlation of errors between trace species. All these molecules are mapped with IASI with better sensitivity owing to its higher spectral resolution and broader spectral range; ozone being retrieved from its strong 9.6 µm band from IASI spectra.

https://doi.org/10.5194/egusphere-2026-805
Preprint. Discussion started: 17 February 2026


## 6 Conclusions

In this paper, we have evaluated the quality of MAJIS spectra acquired in the infrared channel during the 2024 JUICE Earth fly-by using co-located observations from IASI and a forward radiative transfer model, 4A/OP. The two instruments overlap in their spectral coverage in the range 3.6–5.56 µm; IASI having a ∼six times better spectral resolution but ∼ten times larger spatial footprint. Our co-location method filters for cloud contamination as well as solar specular reflection (glint spot). Taking into account strict temporal co-location criteria (less than one hour apart), only three IASI spectra can be compared with MAJIS ones. Once convolved to MAJIS spectral resolution, the IASI spectra are in excellent agreement with MAJIS. A small spectral shift of the order of 4 nm is derived from this comparison, documented in more detail in Langevin et al. (2026). Once this shift is taken into account, we suggest that the residual difference between the two datasets can be attributed to small differences in atmospheric water vapour content that can quickly vary, which highlights the challenge of this inter-comparison exercise. By repeating this comparison to pairs of IASI-MAJIS data acquired up to 2 hours apart, we conclude that the absolute radiometric calibration of MAJIS is better than 10% except beyond 5.25 µm, where MAJIS seems to underestimates the actual radiance by ∼15–20%.

We then used the 4A/OP radiative transfer model together with a reference state of the atmosphere (partly coming from IASI Level 2 data) to compute a synthetic spectrum that best matches the MAJIS observations. The residuals (observations minus forward model) were used to estimate the noise level: the resulting signal-to-noise ratio (SNR), in the range 200–300, meets the nominal expectations from ground-based calibration (Poulet et al., 2025). We further evaluated the sensitivity of MAJIS spectra to several trace species (ozone, methane, carbon monoxide and nitrous oxide), both in terms of vertical domain of sensitivity and minimum level of uncertainty on their total column, if retrievals errors were only due to instrumental noise. This leads to a sensitivity of MAJIS data to a change of 14% in the column of $CH_4$ and CO; 5% in $O_3$ and 2.5% in $N_2O$.

While the near infrared spectrum of the Earth is dominated by water vapour and carbon dioxide, on Jupiter, MAJIS spectra will be dominated by methane bands. Methane, with a volume mixing ratio of 0.2%, is the third most abundant species in Jupiter's atmosphere (after $H_2$ and helium). Other molecules that are expected to be detected and mapped by MAJIS at Jupiter are two condensible species: ammonia (300–400 ppm, condensation level near 800 mbar) and water (0.25% or 2500 ppm in the deep atmosphere, but decreasing sharply above its condensation level near 5 bars), and non-condensible and disequilibrium species : phosphine (∼ppm level), CO, germane and arsine (∼ half a ppb) (Fletcher et al., 2023). It is not possible to link our estimates on the precision level of a given trace species on Earth to future jovian measurements, given the very different gaseous composition, clouds and haze properties between the two planets. The best lesson learned from the Earth fly-by is the assessment of the excellent radiometric calibration and of nominal noise level, which gives confidence that future trace species retrievals on Jupiter will meet expectations. Indeed, similar signal-to-noise ratios (SNR) as those obtained during the Earth fly-by are expected from future Jupiter MAJIS observations (Poulet et al., 2025). The performances of a MAJIS-like instrument regarding the retrieval of trace species have been evaluated by Grassi et al. (2010) and are expected to be slightly better than those from the Jupiter Infrared and Auroral Mapper (JIRAM) instrument onboard Juno, for the same SNR, owing to MAJIS slightly better spectral resolution (6.86 nm versus 9 nm) and spectral coverage extended to 5.4 µm (while JIRAM stops

https://doi.org/10.5194/egusphere-2026-805
Preprint. Discussion started: 17 February 2026


at 5 µm). The main expected improvement regards ammonia retrievals, with foreseen 1-$\sigma$ uncertainty divided by two compared to retrievals from JIRAM, along with greater vertical sensitivity. Ammonia – together with aforementioned disequilibrium species – is an important tracer of vertical motion, both from the large scale circulation and small-scale convective events. Combined with its high spatial resolution and temporal sampling, we expect MAJIS to bring valuable new constraints to Jupiter's tropospheric dynamics and meteorological activity.

*Data availability.* The MAJIS data acquired during the JUICE Moon–Earth flyby in August 2024 are currently under the mission's cruise-phase proprietary period. These data will be made available through the ESA Planetary Science Archive following the first Cruise Archive Delivery, which is currently scheduled for six months after Earth Gravity Assist 3 in 2029.

*Author contributions.* SG led the study, wrote the paper, performed most of the comparisons with IASI observations and the radiative transfer calculations. RA provided the IASI data, developed the radiative transfer algorithm 4A/OP and contributed to the data analysis. NL contributed to the data analysis and visualization. FP, YL and SR participated in the discussion of the results. All authors reviewed and edited the manuscript.

*Competing interests.* The authors have no competing interests to declare.

*Acknowledgements.* French participation to this work on MAJIS data analysis was supported by the Centre National d'Etudes Spatiales (CNES). The Italian participation to JUICE mission is funded by the Italian Space Agency (ASI). In particular, this work has been developed under the ASI-INAF agreement n. 2023-6-HH.0. The Jupiter Icy Moons Explorer is a mission under ESA leadership with contributions from its Member States, NASA, JAXA and the Israel Space Agency. It is the first Large-class mission in ESA's Cosmic Vision programme. IASI has been built under the responsibility of CNES. The authors thank EUMETSAT for providing IASI data through EUMETCast service, and the AERIS data infrastructure for data processing (https://www.aeris-data.fr/). LMD particularly thanks CNES for the long term support of the 4A/OP radiative transfer model.

https://doi.org/10.5194/egusphere-2026-805
Preprint. Discussion started: 17 February 2026


## References

Armante, R., Scott, N., Crevoisier, C., Capelle, V., Crepeau, L., Jacquinet, N., and Chédin, A.: Evaluation of spectroscopic databases through radiative transfer simulations compared to observations. Application to the validation of GEISA 2015 with IASI and TCCON, Journal of Molecular Spectroscopy, 327, 180–192, https://doi.org/10.1016/j.jms.2016.04.004, 2016.

August, T., Klaes, D., Schlüssel, P., Hultberg, T., Crapeau, M., Arriaga, A., O'Carroll, A., Coppens, D., Munro, R., and Calbet, X.: IASI on Metop-A: Operational Level 2 retrievals after five years in orbit, Journal of Quantitative Spectroscopy and Radiative Transfer, 113, 1340–1371, https://doi.org/10.1016/j.jqsrt.2012.02.028, 2012.

Capelle, V., Chédin, A., Siméon, M., Tsamalis, C., Pierangelo, C., Pondrom, M., Crevoisier, C., Crepeau, L., and Scott, N. A.: Evaluation of IASI-derived dust aerosol characteristics over the tropical belt, Atmospheric Chemistry & Physics, 14, 9343–9362, https://doi.org/10.5194/acp-14-9343-201410.5194/acpd-13-30143-2013, 2014.

Capelle, V., Hartmann, J.-M., and Crevoisier, C.: A full physics algorithm to retrieve nighttime sea surface temperature with IASI: Toward an independent homogeneous long time-series for climate studies, Remote Sensing of Environment, 269, 112838, https://doi.org/10.1016/j.rse.2021.112838, 2022.

Cassé, V., Armante, R., Bousquet, P., Chomette, O., Crevoisier, C., Delahaye, T., Edouart, D., Gibert, F., Millet, B., Nahan, F., and Pierangelo, C.: Development and Validation of an End-to-End Simulator and Gas Concentration Retrieval Processor Applied to the MERLIN Lidar Mission, Remote Sensing, 13, 2679, https://doi.org/10.3390/rs13142679, 2021.

Cheruy, F., Scott, N. A., Armante, R., Tournier, B., and Chedin, A.: Contribution to the development of radiative transfer models for high spectral resolution observations in the infrared., Journal of Quantitative Spectroscopy and Radiative Transfer, 53, 597–611, https://doi.org/10.1016/0022-4073(95)00026-H, 1995.

Clerbaux, C., Boynard, A., Clarisse, L., George, M., Hadji-Lazaro, J., Herbin, H., Hurtmans, D., Pommier, M., Razavi, A., Turquety, S., Wespes, C., and Coheur, P.-F.: Monitoring of atmospheric composition using the thermal infrared IASI/MetOp sounder, Atmospheric Chemistry & Physics, 9, 6041–6054, https://doi.org/10.5194/acp-9-6041-200910.5194/acpd-9-8307-2009, 2009.

Crevoisier, C., Chédin, A., Matsueda, H., Machida, T., Armante, R., and Scott, N. A.: First year of upper tropospheric integrated content of $CO_2$ from IASI hyperspectral infrared observations, Atmospheric Chemistry & Physics, 9, 4797–4810, https://doi.org/10.5194/acp-9-4797-200910.5194/acpd-9-8187-2009, 2009.

Crevoisier, C., Nobileau, D., Armante, R., Crépeau, L., Machida, T., Sawa, Y., Matsueda, H., Schuck, T., Thonat, T., Pernin, J., Scott, N. A., and Chédin, A.: The 2007-2011 evolution of tropical methane in the mid-troposphere as seen from space by MetOp-A/IASI, Atmospheric Chemistry & Physics, 13, 4279–4289, https://doi.org/10.5194/acp-13-4279-201310.5194/acpd-12-23731-2012, 2013.

Delahaye, T., Armante, R., Scott, N. A., Jacquinet-Husson, N., Chédin, A., Crépeau, L., Crevoisier, C., Douet, V., Perrin, A., Barbe, A., Boudon, V., Campargue, A., Coudert, L. H., Ebert, V., Flaud, J.-M., Gamache, R. R., Jacquemart, D., Jolly, A., Kwabia Tchana, F., Kyuberis, A., Li, G., Lyulin, O. M., Manceron, L., Mikhailenko, S., Moazzen-Ahmadi, N., Müller, H. S. P., Naumenko, O. V., Nikitin, A., Perevalov, V. I., Richard, C., Starikova, E., Tashkun, S. A., Tyuterev, V. G., Vander Auwera, J., Vispoel, B., Yachmenev, A., and Yurchenko, S.: The 2020 edition of the GEISA spectroscopic database, Journal of Molecular Spectroscopy, 380, 111510, https://doi.org/10.1016/j.jms.2021.111510, 2021.

Dogniaux, M., Crevoisier, C., Armante, R., Capelle, V., Delahaye, T., Cassé, V., De Mazière, M., Deutscher, N. M., Feist, D. G., Garcia, O. E., Griffith, D. W. T., Hase, F., Iraci, L. T., Kivi, R., Morino, I., Notholt, J., Pollard, D. F., Roehl, C. M., Shiomi, K., Strong, K., Té, Y., Velazco, V. A., and Warneke, T.: The Adaptable 4A Inversion (5AI): description and first $X_{CO<SUB>2}$</SUB> retrievals from Orbiting Carbon

https://doi.org/10.5194/egusphere-2026-805
Preprint. Discussion started: 17 February 2026


Observatory-2 (OCO-2) observations, Atmospheric Measurement Techniques, 14, 4689–4706, https://doi.org/10.5194/amt-14-4689-2021, 2021.

Fletcher, L. N., Cavalié, T., Grassi, D., Hueso, R., Lara, L. M., Kaspi, Y., Galanti, E., Greathouse, T. K., Molyneux, P. M., Galand, M., Vallat, C., Witasse, O., Lorente, R., Hartogh, P., Poulet, F., Langevin, Y., Palumbo, P., Gladstone, G. R., Retherford, K. D., Dougherty, M. K., Wahlund, J.-E., Barabash, S., Iess, L., Bruzzone, L., Hussmann, H., Gurvits, L. I., Santolik, O., Kolmasova, I., Fischer, G., Müller-Wodarg, I., Piccioni, G., Fouchet, T., Gérard, J.-C., Sánchez-Lavega, A., Irwin, P. G. J., Grodent, D., Altieri, F., Mura, A., Drossart, P., Kammer, J., Giles, R., Cazaux, S., Jones, G., Smirnova, M., Lellouch, E., Medvedev, A. S., Moreno, R., Rezac, L., Coustenis, A., and Costa, M.: Jupiter Science Enabled by ESA's Jupiter Icy Moons Explorer, Space Science Reviews, 219, 53, https://doi.org/10.1007/s11214-023-00996-6, 2023.

Grassi, D., Adriani, A., Moriconi, M. L., Ignatiev, N. I., D'Aversa, E., Colosimo, F., Negrão, A., Brower, L., Dinelli, B. M., Coradini, A., and Piccioni, G.: Jupiter's hot spots: Quantitative assessment of the retrieval capabilities of future IR spectro-imagers, Planetary and Space Sciences, 58, 1265–1278, https://doi.org/10.1016/j.pss.2010.05.003, 2010.

Guérin, C.-A., Capelle, V., and Hartmann, J.-M.: Revisiting the Cox and Munk wave-slope statistics using IASI observations of the sea surface, Remote Sensing of Environment, 288, 113508, https://doi.org/10.1016/j.rse.2023.113508, 2023.

Haffoud, P., Poulet, F., Vincendon, M., Filacchione, G., Barbis, A., Guiot, P., Lecomte, B., Langevin, Y., Piccioni, G., Dumesnil, C., Rodriguez, S., Carter, J., Stefania, S., Tommasi, L., Tosi, F., and Pilorget, C.: Calibration of MAJIS (Moons And Jupiter Imaging Spectrometer). III. Spectral calibration, Review of Scientific Instruments, 95, 031301, https://doi.org/10.1063/5.0188944, 2024.

Jacquinet-Husson, N., Armante, R., Scott, N. A., Chédin, A., Crépeau, L., Boutammine, C., Bouhdaoui, A., Crevoisier, C., Capelle, V., Boonne, C., Poulet-Crovisier, N., Barbe, A., Chris Benner, D., Boudon, V., Brown, L. R., Buldyreva, J., Campargue, A., Coudert, L. H., Devi, V. M., Down, M. J., Drouin, B. J., Fayt, A., Fittschen, C., Flaud, J.-M., Gamache, R. R., Harrison, J. J., Hill, C., Hodnebrog, Ø., Hu, S.-M., Jacquemart, D., Jolly, A., Jiménez, E., Lavrentieva, N. N., Liu, A.-W., Lodi, L., Lyulin, O. M., Massie, S. T., Mikhailenko, S., Müller, H. S. P., Naumenko, O. V., Nikitin, A., Nielsen, C. J., Orphal, J., Perevalov, V. I., Perrin, A., Polovtseva, E., Predoi-Cross, A., Rotger, M., Ruth, A. A., Yu, S. S., Sung, K., Tashkun, S. A., Tennyson, J., Tyuterev, V. G., Vander Auwera, J., Voronin, B. A., and Makie, A.: The 2015 edition of the GEISA spectroscopic database, Journal of Molecular Spectroscopy, 327, 31–72, https://doi.org/10.1016/j.jms.2016.06.007, 2016.

Langevin, Y., Rodriguez, S., Poulet, F., Guerlet, S., Armante, R., Agostini, L., D'Aversa, E., Royer, C., Fletcher, L., Oliva, F., Seignovert, B., Stephan, K., and Tosi, F.: Post-launch spectral and radiometric performances of MAJIS, the VIS–NIR imaging spectrometer of JUICE, EGUsphere, 2026, 2026.

Larar, A. M., Smith, W. L., Zhou, D. K., Liu, X., Revercomb, H., Taylor, J. P., Newman, S. M., and Schlüssel, P.: IASI spectral radiance validation inter-comparisons: case study assessment from the JAIVEx field campaign, Atmospheric Chemistry & Physics, 10, 411–430, https://doi.org/10.5194/acp-10-411-201010.5194/acpd-9-10193-2009, 2010.

Oliva, F., D'Aversa, E., Migliorini, A., Piccioni, G., Poulet, F., Langevin, Y., Filacchione, G., Ciarniello, M., Rodriguez, S., Seignovert, B., Mura, A., Fletcher, L. N., Zinzi, A., Giardino, M., Lopinto, E., Sindoni, G., and Plainaki, C.: JUICE-MAJIS Earth observations during the 2024 gravity assist: first analysis and comparison with PRISMA data, EGUsphere, 2026, 1–51, https://doi.org/10.5194/egusphere-2025-6455, 2026.

Phulpin, T., Blumstein, D., Prel, F., Tournier, B., Prunet, P., and Schlüssel, P.: Applications of IASI on MetOp-A: first results and illustration of potential use for meteorology, climate monitoring, and atmospheric chemistry, in: Atmospheric and Environmental Remote Sensing Data Processing and Utilization III: Readiness for GEOSS, edited by Goldberg, M. D., Bloom, H. J., Huang, A. H., and Ardanuy, P. E.,

https://doi.org/10.5194/egusphere-2026-805
Preprint. Discussion started: 17 February 2026


vol. 6684 of *Society of Photo-Optical Instrumentation Engineers (SPIE) Conference Series*, p. 66840F, https://doi.org/10.1117/12.736816, 2007.

Poulet, F., Piccioni, G., Langevin, Y., Dumesnil, C., Tommasi, L., Carlier, V., Filacchione, G., Amoroso, M., Arondel, A., D'Aversa, E., Barbis, A., Bini, A., Bolsée, D., Bousquet, P., Caprini, C., Carter, J., Dubois, J.-P., Condamin, M., Couturier, S., Dassas, K., Dexet, M., Fletcher, L., Grassi, D., Guerri, I., Haffoud, P., Larigauderie, C., Le Du, M., Mugnuolo, R., Pilato, G., Rossi, M., Stefani, S., Tosi, F., Vincendon, M., Zambelli, M., Arnold, G., Bibring, J.-P., Biondi, D., Boccaccini, A., Brunetto, R., Carapelle, A., Cisneros González, M., Hannou, C., Karatekin, O., Le Cle'ch, J.-C., Leyrat, C., Migliorini, A., Nathues, A., Rodriguez, S., Saggin, B., Sanchez-Lavega, A., Schmitt, B., Seignovert, B., Sordini, R., Stephan, K., Tobie, G., Zambon, F., Adriani, A., Altieri, F., Bockelée, D., Capaccioni, F., De Angelis, S., De Sanctis, M.-C., Drossart, P., Fouchet, T., Gérard, J.-C., Grodent, D., Ignatiev, N., Irwin, P., Ligier, N., Manaud, N., Mangold, N., Mura, A., Pilorget, C., Quirico, E., Renotte, E., Strazzulla, G., Turrini, D., Vandaele, A.-C., Carli, C., Ciarniello, M., Guerlet, S., Lellouch, E., Mancarella, F., Morbidelli, A., Le Mouélic, S., Raponi, A., Sindoni, G., and Snels, M.: Moons and Jupiter Imaging Spectrometer (MAJIS) on Jupiter Icy Moons Explorer (JUICE), Space Science Reviews, 220, 27, https://doi.org/10.1007/s11214-024-01057-2, 2024.

Poulet, F., Piccioni, G., Langevin, Y., Dumesnil, C., Carlier, V., Seignovert, B., Dexet, M. a nd N. Fletcher, L., Leyrat, C., Altieri, F., Carter, J., D'Aversa, E., De Sanctis, M., Grassi, D., Gu erlet, S., Le Mouélic, S., Migliorini, A., Oliva, F., Royer, C., Rodriguez, S., Stephan, K., Tosi, F., Zambon, F., Adriani, A., Arnold, G., Bibring, J.-P., Bockelée, D., Brunetto, R., Capaccioni, F., Carli, C., Cavalié, T., Cisneros González, M., Ciarnello, M., De Angelis, S., Drossart, P., Fil acchione, G., Fouchet, T., Gérard, J.-C., Grodent, D., Irwin, P., Jacquinod, S., Karatekin, O., Lel louch, E., Ligier, N., Mangold, N., Mebsout, M., Merlin, F., Morbidelli, A., Mura, A., Nathues, A. an d E. Palumbo, M., Pilorget, C., Poch, O., Quirico, E., Raponi, A., Robert, S., Roussos, E., Sanchez-L avega, A., Schmitt, B., Sindoni, G., Snels, M., Sordini, R., Stefani, S., Strazzulla, G., Trent, T. a nd Tobie, G., Turrini, D., Vandaele, A.-C., Vincendon, M., Witasse, O., Vallat, C., and Moraino, A.: ESA/JUICE encounters Earth/Moon in 2024: overview of the Moons And Jupiter Imaging Spectrometer (MAJIS) observati ons, EGUsphere, 2025, 1–58, https://doi.org/10.5194/egusphere-2025-6191, 2025.

Scott, N. A. and Chedin, A.: A fast line-by line method for atmospheric absorption computations: the Automatized Atmospheric Absorption Atlas., Journal of Applied Meteorology, 20, 802–812, https://doi.org/10.1175/1520-0450(1981)020<0802:AFLBLM>2.0.CO;2, 1981.

Sic, B., Jacquette, E., Jouglet, D., Lafrique, P., Pierangelo, C., Armante, R., Lezeaux, O., and Hajj, M. E.: Implementation of low stream interpolation technique to accelerate scattering calculations in the 4A/OP radiative transfer model, Journal of Quantitative Spectroscopy and Radiative Transfer, 349, 109734, https://doi.org/10.1016/j.jqsrt.2025.109734, 2026.

Tosi, F., Royer, C., Colaiuta, F., Poulet, F., Powell, T. M., Greenhagen, B. T., Langevin, Y., Mura, A., Piccioni, G., Pilorget, C., Carli, C., and Zambon, F.: The JUICE 2024 close flyby of the Moon: Thermal assessment from MAJIS, EGUsphere, 2025, 1–43, https://doi.org/10.5194/egusphere-2025-6150, 2025.